

Pb₂MgXO₆ (X = W and Te) Double Perovskites: New Insights into Their Electronic, Elastic, Optic and Thermoelectric Properties

M. FODIL^{a,b,*}, O. BARAKA^{a,c} AND A. MOKADEM^d

^aFaculty of Science and Technology, Hassiba Benbouali University, No. 19, Chlef, 02000, Algeria

^bLaboratory Physico-Chemistry of Advanced Materials, Djilali Liabes University, BP 89, 22000, Sidi Bel Abbes, Algeria

^cLaboratory Optical Materials and Devices, Djilali Liabes University, BP 89, 22000, Sidi Bel Abbes, Algeria

^dNationale Polytechnique Institut of Oran, B.P. 1523 El M'Naouer, 31000, Oran, Algeria

Received: 03.03.2024 & Accepted: 20.05.2024

Doi: [10.12693/APhysPolA.146.143](https://doi.org/10.12693/APhysPolA.146.143)

*e-mail: m.fodil@univ-chlef.dz

We carried out a theoretical study in which we explored the mechanical, optoelectronic, and thermoelectric properties of Pb₂Mg(W/Te)O₆ double perovskites with first-principles density functional approach and Boltzmann transport theory. The calculations were performed with the Perdew–Burke–Ernzerhof generalized gradient approximation and the Heyd–Scuseria–Ernzerhof functional (HSE06). Examination of structural stability is conducted through the analysis of the tolerance factor. The analysis of elastic constants within generalized gradient approximations reveals that both compounds satisfy the Born stability criteria and have excellent machinability. Moreover, they have a ductile nature with metallic bonding and a low Debye temperature. The examined materials possessed a significant effective mass in both compounds and direct bandgaps with values 2.4 eV (3.7 eV) for Pb₂MgWO₆ and 2.7 eV (4.2 eV) for Pb₂MgTeO₆ obtained within Perdew–Burke–Ernzerhof generalized gradient approximation (hybrid HSE06), respectively. Therefore, Pb₂Mg(W/T)O₆ demonstrates different photovoltaic capabilities with a low power conversion efficiency of ~ 10% employing HSE06, which are the appropriate attributes for the solar cell photoelectric absorption layers. Furthermore, the examined materials have excellent substantial thermopower, as well as figures of merit of 2.46 (2.67) and 2.26 (2.47) for Pb₂MgTeO₆ and Pb₂MgWO₆, respectively, ensuring the appropriate application for thermoelectric devices.

topics: perovskites, effective masses, hybrid functional HSE06, optoelectronics properties

1. Introduction

In recent years, researchers have observed a growing interest in studying transition metal oxides with an ordered double perovskite structure. Perovskite materials can display various properties [1–11] of electronic structures (insulating, semiconducting, metallic, and half-metallic with spin-polarized electrical conductivity). Some perovskite materials demonstrate superconductivity, various magnetic orderings (antiferromagnetic, ferri-, and ferromagnetic), and high ionic conductivity, which qualifies them for use in solid oxide fuel cells. They also possess catalytic activity, enabling their use in chemical reactions and environmental remediation processes. Perovskites can have distinct functional features due to atomic displacements, thanks to which they are ferroelectric, magnetic-dielectric, and multiferroic.

A significant amount of research focused on enhancing the properties of these perovskite substances has resulted in the development of double perovskites with the stoichiometry A₂BB'X₆ [12]. The double perovskite (DP) oxide family with a stoichiometry of A₂BB'O₆ [13–15] has significantly increased its advantage in various technological applications [7–11, 16], including solar cells, electronic devices (transistors, diodes, and light-emitting diodes), magnetic devices (magnetic memory components and data storage devices), and piezoelectric devices (actuators, sensors, and transducers), sensors (for detecting gases, humidity, and light), catalysis (in chemical synthesis, pollution control, and energy conversion processes), and energy storage (in batteries and supercapacitors).

The properties of perovskite materials can be tailored through partial substitutions and variations in synthesis methods, allowing for customization to suit specific applications.

The current research demonstrates significant findings regarding the properties of certain materials. Specifically, it emphasizes the discovery of substantial magnetoresistance and half metallicity in $\text{Sr}_2\text{FeMoO}_6$ and $\text{Sr}_2\text{FeReO}_6$ [17, 18] at room temperature. Additionally, the study reveals the presence of superconductivity in $\text{A}_2\text{Os}_2\text{O}_7$ [19], where A represents Cs, Rb, and K. Furthermore, the study identifies the existence of half semi-metallic antiferromagnetism in $\text{Sr}_2\text{CrOsO}_6$ [20]. In solar cells, $\text{Ba}_2\text{BiSbO}_6$ [21] shows great promise as a photon absorber material. In addition to its photoluminescent abilities, Sr_2CrWO_6 [22] is also a photocatalyst. Additionally, Ba_2YMoO_6 [23] is used in devices that efficiently transform energy. These are just a sampling of the numerous double perovskite compounds that exist, each with its own unique set of characteristics and possible uses. The fast growth of double perovskite research may be attributed to the growing need for novel materials with improved functionalities and performance across a wide range of technological applications.

According to the findings of empirical research, $\text{Pb}_2\text{MgTeO}_6$, when heated to high temperatures, takes on a structure that is a face-centered cubic structure. The temperature at which the transition from $Fm-3m$ [Phase 1] to $R3m$ [Phase 2] takes place is around 194 K, whereas the transition from $R3m$ to $R3$ [Phase 3] takes place at approximately 142 K [24, 25]. Using *ab initio* calculations, R. Caracas and X. Gonze [26] characterized the cubic phase and the rhombohedral phase equilibrium states of $\text{Pb}_2\text{MgTeO}_6$ (PMT). Besides, they established the dynamical features corresponding to both phases [27]. An investigation of the antiferroelectric material Pb_2MgWO_6 was carried out using neutron diffraction [28]. The experiment was conducted under a pressure of 5.4 GPa, maintaining room temperature. The results supported the conclusions reached by Baldinozzi et al. [29] in their earlier research.

Few properties have been demonstrated by earlier studies, making these materials more promising than others and an excellent choice for further investigation in the hope of discovering intriguing properties. We decided to examine the electronic structures, elastic characteristics, and optical and thermoelectric properties. This is achieved by using the *ab initio* method. As a result, our research will provide fresh perspectives on energy systems.

2. Theoretical method

The implementation of the WIEN2k code of the full-potential linearized augmented plane wave technique [30, 31], based on density functional theory (DFT) [32], was utilized in the computations. The $\text{Pb}_2\text{Mg}(\text{W}/\text{Te})\text{O}_6$'s structural characteristics were obtained using the the generalized

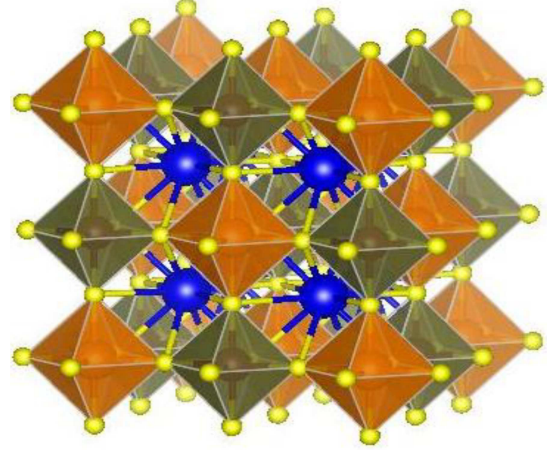


Fig. 1. Schematic of the Pb_2MgXO_6 ($X = \text{W}$ and Te) double perovskites crystal structure.

gradient approximation (PBE-GGA) potential [33]. Additionally, the bandgap was calculated precisely using the hybrid Heyd–Scuseria–Ernzerhof technique (HSE06) [34], which avoids the pitfall of the PBE approach by correctly estimating the bandgap. To avoid any overlapping of the muffin-tin spheres, the corresponding R_{MT} values were adjusted to 2.3 a.u for Pb, 1.8 a.u for Mg (W/Te), and 1.5 a.u for O. It was decided that $R_{MT}k_{\text{max}}$ would be 9.0 (R_{MT} denotes the smallest muffin-tin radius in the unit cell, and the maximum value of the reciprocal lattice vector is denoted by k_{max}) to ensure the reliability of our results. We used the largest wave vector value $G_{\text{max}} = 12$ and the cut-off for the angular functions $l_{\text{max}} = 10$, and 1000 k-points ($10 \times 10 \times 10$ mesh grids) were employed to generate the irreducible Brillouin zone (IBZ). The self-consistent convergence of the total energy was set to 10^{-3} Ry. Using the stress-strain approach, the cubic single-crystal elastic constants C_{ij} were determined [35]. For interband optical transitions, the matrix components are taken into consideration; it is the ideal solution to derive all of the optical characteristics from the complex dielectric function $\varepsilon(\omega) = \varepsilon_1(\omega) + i\varepsilon_2(\omega)$. Thermoelectric properties were analyzed using the BoltzTraP program [36], based on classical transport theory.

3. Results and discussion

3.1. Material and structural stability

Figure 1 shows the cubic structures of $\text{Pb}_2\text{Mg}(\text{W}/\text{Te})\text{O}_6$ with space group $Fm-3m$, which is characterized by lattice parameters $a = b = c$, indicating isotropic photoelectric characteristics in x , y , and z directions. Here, WO_6 and TeO_6 form an octahedron with shared corners, in

TABLE I

Structural parameters of double perovskite Pb_2MgTeO_6 and Pb_2MgWO_6 .

Crystal structure parameters	Pb_2MgTeO_6 [25]	Pb_2MgWO_6 [28]
Space group	$Fm-3m$	$Fm-3m$
Lattice constants		
a [Å]	7.99	8.0058
Unit cell volume		
V [Å ³]	510	512.9
Oxygen coordinate		
O ($u, 0, 0$)	0.26	0.24
Tolerance factor		
τ	1.0	0.97

which the Pb-site cations occupy interstitial areas. At ambient temperatures, the occupied Wyckoff positions of lead, magnesium, tellurium/tungsten, and oxygen are 8c (1/4, 1/4, 1/4), 4a (0, 0, 0), 4b (1/2, 1/2, 1/2), and 24e (0, 0, u), respectively. Calculations are carried out with experimental parameters, using empirical lattice constants and oxygen coordinate values (see Table I and [25, 28]).

In order to resolve the crystal stability of the compounds under consideration, we evaluate the tolerance factor using Goldschmidt's empirical criteria [37]. The concept of the tolerance factor can be adapted to double perovskites as well. In general, for double perovskites with mixed B-site, the tolerance factor is defined as [38, 39]

$$\tau = \frac{x_A + x_O}{\sqrt{2} \left(\frac{x_B + x_{B'}}{2} + x_O \right)}, \quad (1)$$

with x_A , x_B , $x_{B'}$, and x_O being the ionic radii of the respective ions. The tolerance factor τ between 0.9–1.0 possesses an ideal cubic structure [40] for the compound. Moreover, the octahedral factor is defined as $\mu = R_B/R_O$, and stable structures tend to have $\mu > 0.41$ [41]. In order to assess these parameters, we employ the effective ionic radii of Shannon [42]. Consequently, the resulting values are $\mu = 0.56$ and $\tau = (0.97/1.0)$ for $Pb_2Mg(W/Te)O_6$, which indicates a stable cubic structure of these compounds.

3.2. Mechanical properties

Theoretical calculations of the elastic constants let us estimate critical technological properties for our perovskite compounds, including stability, hardness, stiffness, brittleness, ductility, and bond nature. They are used to determine mechanical properties. The double perovskite compounds have a face-centered cubic structure with three elasticity parameters: C_{11} , C_{12} , and C_{44} . All of the elastic

TABLE II

The computed values of elastic and mechanical parameters for Pb_2MgXO_6 ($X = Te$ and W) double perovskite compounds.

Parameter	Unit	Pb_2MgTeO_6	Pb_2MgWO_6
a	[Å]	7.99	8.00
C_{11}	[GPa]	217.971	197.517
C_{12}	[GPa]	136.475	159.820
C_{44}	[GPa]	47.525	40.909
E	[GPa]	122.877	82.771
B	[GPa]	163.640	172.386
G	[GPa]	44.687	29.974
ν		0.375	0.418
A		1.17	2.17
B/G		3.66	5.75
H_V^{Tian}	[GPa]	3.10	1.40
C_p	[GPa]	88.95	118.91
$T_{melt} \pm 300$	[K]	1841.4	1720.5
ς		0.72	0.86
ρ	[g/cm ³]	8.64	9.30
v_m	[m/s]	2565.02	2037.06
v_l	[m/s]	5081.76	4778.04
v_s	[m/s]	2273.71	1795.13
θ_D	[K]	327.12	259.08

constants for our compounds are listed in Table II. Positive elastic energy or an elastic stiffness matrix that satisfies the well-known Born stability criteria are prerequisites for a crystal to be mechanically stable. The criteria impose the following conditions for cubic structures: $C_{11} + 2C_{12} > 0$, $C_{11} - C_{12} > 0$, and $C_{44} > 0$ [43]. Our results satisfy these conditions, showing that our compounds are mechanically stable. Utilizing the equations listed in this section, the mechanical properties such as bulk modulus (B), shear modulus (G), Young's modulus (E), anisotropy factor (A), Pugh's ratio (B/G), Cauchy pressure (C_p), Poisson's ratio (ν), Kleinman parameter (ς), etc., were calculated and listed in Table II.

The bulk modulus (B) and shear modulus (G) were computed using Voigt's and Reuss' approximation [44], namely

$$B = \frac{1}{3} (C_{11} + 2C_{12}), \quad (2)$$

$$G = \frac{1}{2} (G_V + G_R). \quad (3)$$

In order to quantify the elastic reply of a substance under hydrostatic pressure, the bulk modulus assesses the resistance to volume change in solids. As an alternative, the resistance to plastic deformation and the stiffness of materials can be measured using shear modulus (G) and Young's modulus (Y), respectively. Table II shows that Pb_2MgTeO_6 has a higher shear modulus value than Pb_2MgWO_6 ,

demonstrating that $\text{Pb}_2\text{MgTeO}_6$ is the hardest compound. The bulk-to-shear modulus ratio is often considered a criterion for assessing brittle properties [45]. The crucial value is 1.75; if higher, the material is considered to be ductile. The calculated B/G values for $\text{Pb}_2\text{MgTeO}_6$ and Pb_2MgWO_6 are 3.66 and 5.75, respectively, suggesting that our substances are erect to be ductile in nature. The Young's modulus (E) can be computed using the relation [38]

$$E = \frac{9GB}{G + 3B}. \quad (4)$$

It can be observed that $\text{Pb}_2\text{MgTeO}_6$ has the value $E = 122.877$ GPa, which indicates that it is significantly stiffer than Pb_2MgWO_6 . The parameter known as the anisotropy factor (A) determines whether or not the material's physical properties are similar in all directions. This parameter must equal 1 for the medium to be considered isotropic; otherwise, the medium is anisotropic. It can be computed using the relation [38]

$$A = \frac{2C_{44}}{C_{11} - C_{12}}. \quad (5)$$

According to Table II, the estimated value deviates from 1 and is more than 1, indicating the elastic anisotropy behavior in our compounds. The indication of Cauchy pressure can be used to identify the type of bond in the structure, and it is defined as

$$C_p = C_{12} - C_{44}. \quad (6)$$

Positive values of C_p indicate non-directional metallic bonding, while negative values indicate directional covalent bonding. The fact that the result was positive suggests that our compounds have non-directional metallic bonding. Poisson's ratio (ν) predicts the brittleness/ductility and type of atomic bonding nature in structure. Under tensile stress, it is the ratio of transverse strain to longitudinal strain. It is a crucial parameter for estimating the failure status of solids and is given by [44]

$$\nu = \frac{1}{2} \frac{(B - \frac{2}{3}G)}{(B + \frac{1}{3}G)}. \quad (7)$$

Frantsevich et al. [46] suggested a specified value of 0.26 to distinguish between ductile and brittle materials. For brittle substantial with covalent bonds, the amount will be less than 0.26. However, the material is considered ductile due to metallic bonding. Our calculated values for $\text{Pb}_2\text{MgTeO}_6$ and Pb_2MgWO_6 are 0.375 and 0.418, respectively. The reported value of ν demonstrates our compounds' ductile nature with metallic bonding, which the Cauchy pressure proved. The capacity to which a substance can resist altering shape serves as a measure of its hardness. The following Tian's equation is used to determine these compounds' exact hardness [47]

$$H_V^{\text{Tian}} = 0.92 \left(\frac{G}{B}\right)^{1.137} G^{0.708}. \quad (8)$$

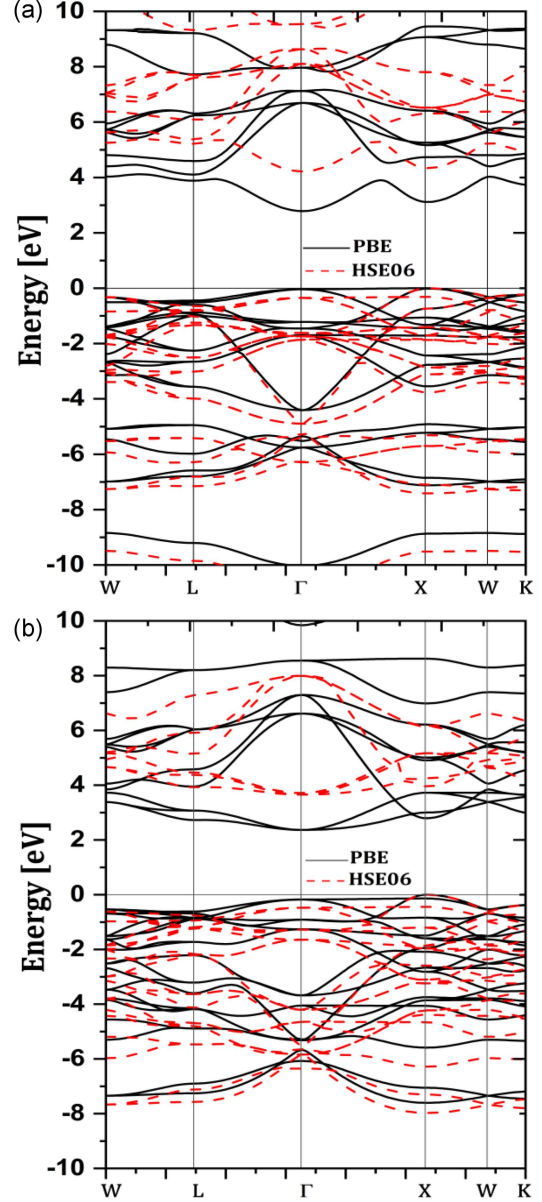


Fig. 2. Band structures of (a) $\text{Pb}_2\text{MgTeO}_6$ and (b) Pb_2MgWO_6 double perovskites.

The calculated hardness values show that $\text{Pb}_2\text{MgTeO}_6$ is a harder compound than Pb_2MgWO_6 .

The thermodynamic parameters, which include the Debye temperatures, sound velocities (v_m), longitudinal velocity (v_l), and transverse velocity (v_s), averaged over the materials under study, are also being researched. The average sound velocity (v_m) serves to estimate the Debye temperature using [48]

$$\theta_D = \frac{h}{k_B} \left[\frac{3n N_A \rho}{4\pi M} \right]^{1/3} v_m. \quad (9)$$

Here, the parameters h , k_B , ρ , and N_A are Planck's constant, Boltzmann's constant, density, and Avogadro's number, respectively, and M is molecular

TABLE III

The computed bandgap and effective mass values of Pb_2MgXO_6 ($X = W$ and Te).

Compound	Bandgap [eV]		Effective mass				Ref.
	PBE	HSE06	PBE		HSE06		
			m_e^*	m_h^*	m_e^*	m_h^*	
Pb_2MgWO_6	2.36	3.656	27.92	-37.17	26.56	-34.93	this work
Pb_2MgTeO_6	2.78	4.21	5.30	-34.71	4.68	-25.80	this work
	3.0						[28]
	2.6						[25]

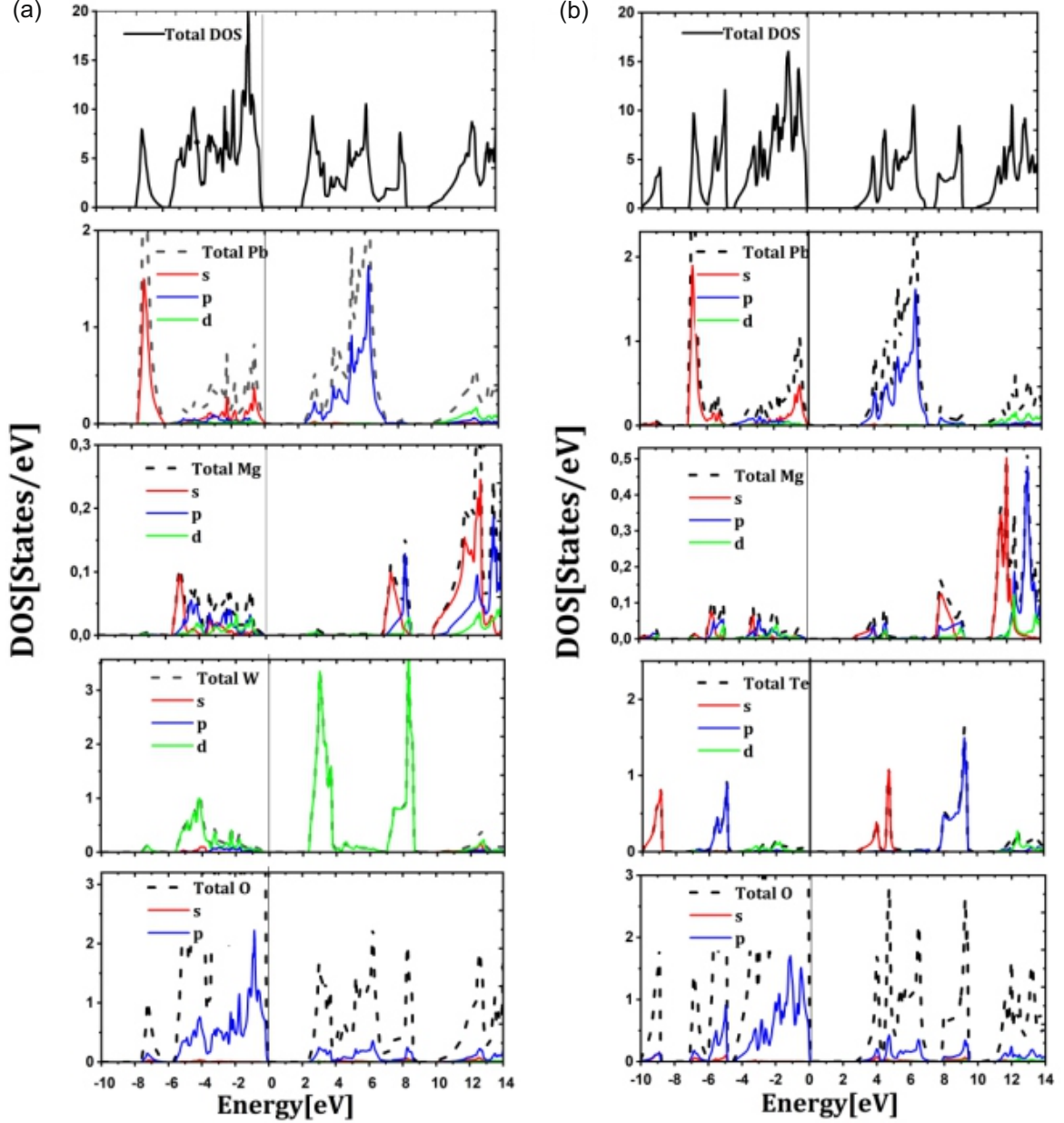


Fig. 3. The computed total density of states (DOS) and partial densities of states of (a) Pb_2MgWO_6 and (b) Pb_2MgTeO_6 double perovskites using the GGA approach.

weight. The bulk modulus B and shear modulus G of a polycrystalline material determine the longitudinal and transverse elastic wave velocities (v_l

and v_s), respectively. The average sound velocity for materials could be determined by employing the subsequent equations [48]

$$v_m = \left[\frac{1}{3} (2/v_s^3 + 1/v_l^3) \right]^{-1/3}, \quad (10)$$

$$v_l = \sqrt{(B + \frac{4}{3}G) / \rho}, \quad (11)$$

$$v_s = \sqrt{G/\rho}. \quad (12)$$

The results are reported in Table II. The values of Debye temperature θ_D for $\text{Pb}_2\text{MgTeO}_6$ and Pb_2MgWO_6 are 327.12 K and 259.08 K, respectively. The Debye temperature is associated with lattice vibrations, which play a role in determining thermal stability. Therefore, $\text{Pb}_2\text{MgTeO}_6$ can withstand extreme heat due to lattice vibrations. The melting temperature is another thermodynamic parameter that has been determined with the empirical formulation [49]

$$T_{\text{melt}}[\text{K}] = (553 + 5.911 C_{11}) \pm 300. \quad (13)$$

The estimated melting temperature is 1841.427 K for $\text{Pb}_2\text{MgTeO}_6$ and 1720.523 K for Pb_2MgWO_6 . Consequently, our compounds are ideal for high-temperature applications due to the higher melting temperature values.

3.3. Electronic properties

Regarding solar cell photoelectric conversion with Pb_2MgWO_6 and $\text{Pb}_2\text{MgTeO}_6$ double perovskite, the compound's electrical structure is an essential factor affecting its light absorption spectra. However, Fig. 2 depicts the band structures of double perovskites with the PBE functional, revealing direct gaps betwixt the lowest (in the conduction bands) and highest (in the valence bands) energy levels in the Γ direction. The values of the energy gaps are listed in Table III (see also [25, 28]). The compounds under consideration do not possess any experimental values. To achieve a more accurate determination of the bandgap, the HSE06 approach is employed. The utilization of the HSE06 method yields bandgap values that exhibit more concurrence with experimental findings when contrasted with those acquired by the GGA approach. The findings show that $\text{Pb}_2\text{MgTeO}_6$ and Pb_2MgWO_6 possess bandgap values of 2.36 eV and 3.78 eV, respectively.

The parabolic approximation of the dispersion band at the lowest conduction and the highest valence bands is employed to calculate the effective masses of photocarriers [50]

$$m^* = \hbar^2 \left[\frac{\partial^2 \gamma(k)}{\partial k^2} \right]^{-1}. \quad (14)$$

Increasing the atomic size of tungsten leads to the inclusion of more impurities, increasing charge carriers. The remarkable carrier mobility exhibited by the compound suggests a strong potential for achieving excellent performance in optoelectronic devices. Figure 3 depicts the energy-dependent

densities of states for the double perovskite Pb_2MgXO_6 ($X = \text{Te}$ and W) compounds. These densities of states were estimated using the PBE-GGA method and are presented within the energy extend for -10 to 14 eV. In the valence band, two distinct peaks in the low energy bands, located approximately at -7 and -5.5 eV, be ascribed to the (Pb) s -states and the (Te/W) p/d -states, respectively. In contrast, the p -states of O atoms, specifically around -5 eV and the Fermi level, are the main central origin of the valence band. However, in the conduction band, the higher energy from 2 to 4 eV is mainly composed of the (W) d -states. Furthermore, both (Te/W) d -states and (O) p -states energy part dominate from values 6 to 9 eV.

3.4. Thermoelectric properties

Thermoelectric (TE) material's performance is measured in terms of the figure of merit (ZT), calculated as $ZT = \frac{\sigma S^2}{k} T$. The parameters S , σ , k , and T are, respectively, the Seebeck coefficient, electrical conductivity, thermal conductivity, and temperature. The figure of merit is an important parameter to detect the type of charge carriers and the optimal doping concentration of materials, as well as the optimal thermal range to obtain high efficiency.

The dependence of S , k , σ , PF as a function of chemical potential (μ) and temperature (T) is displayed in Fig. 4. We have defined the characteristics of both p-type and n-type behaviors. The electronic results show more accessible states in the valence band than in the conduction band, which corresponds to a large number of hole carriers that reinforce the p-type character of the examined materials [51]. The Seebeck coefficient S is an important quantity characterizing the potential (V) between two dissimilar electrical conductors when their temperatures T diverge between them. The coefficient S illustrated in Fig. 4a and e is related to the chemical potential and temperature, respectively.

In the HSE06 method, the large bandgap and flat conduction band around the Fermi level are responsible for the increased Seebeck coefficient. Based on the results from the PBE (HSE06) method, the highest values for the Seebeck coefficient in $\text{Pb}_2\text{MgTeO}_6$ and Pb_2MgWO_6 are 1.02 (1.0) mV/K and 0.10 (0.93) mV/K, respectively. Moreover, Seebeck coefficient versus temperature T [K] was plotted in Fig. 4e for the $\text{Pb}_2\text{Mg}(\text{Te/W})\text{O}_6$ materials, the GGA approximation reveals the value ($3.19 \times 10^{-5}/8.34 \times 10^{-5}$) V/K at 200 K, which increases to ($1.10 \times 10^{-4}/1.66 \times 10^{-4}$) V/K at 1600 K. However, the value at 1600 K reduces by 0.1 when using the HSE06 method.

The calculated values of conductivity, determined using the GGA (HSE06) approximation, are depicted in Fig. 4c and f. For Pb_2MgWO_6 , the maximum value of the parameter σ is observed to be

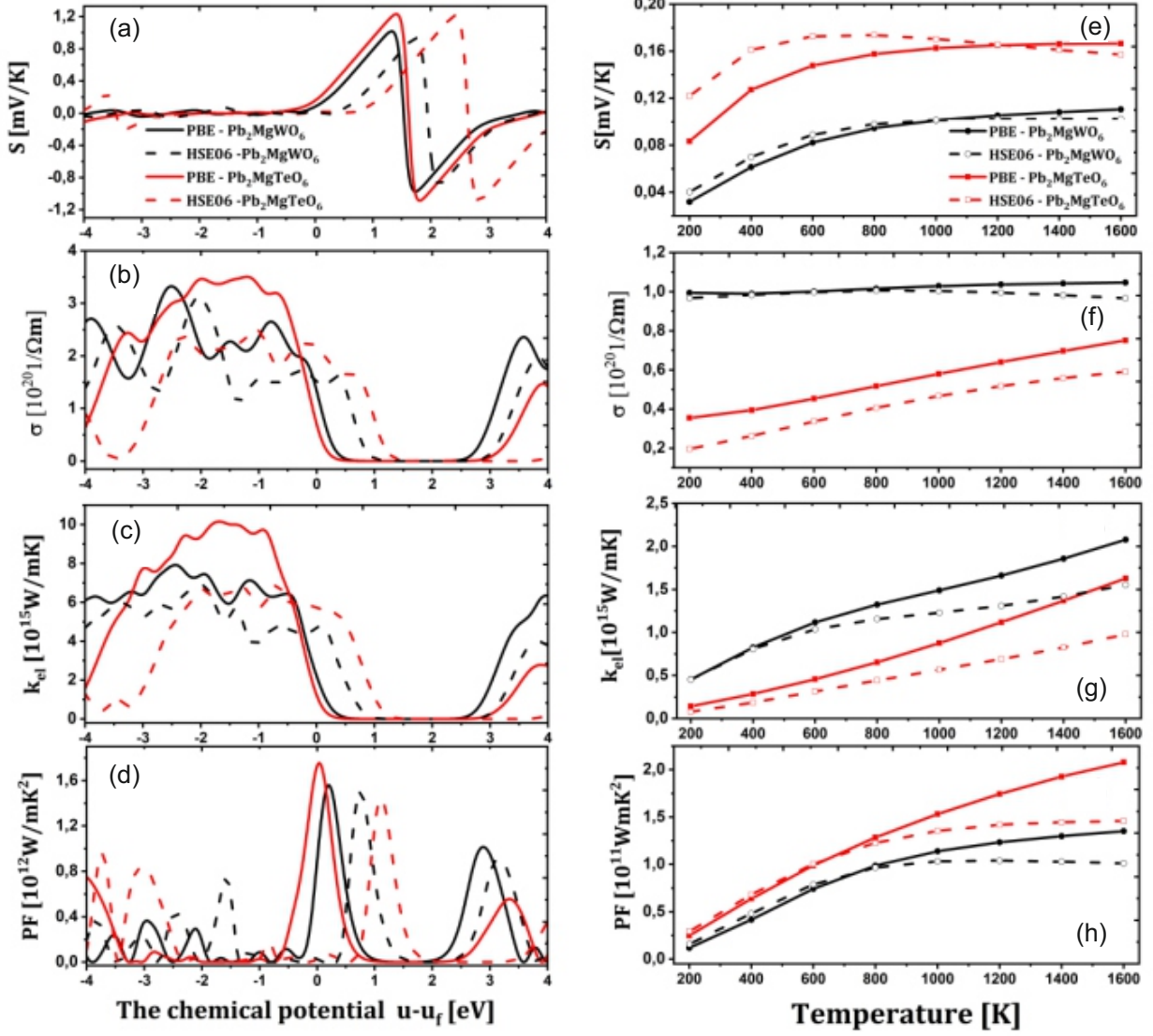


Fig. 4. Calculated thermoelectric parameters as a function of chemical potential and temperature.

3.3×10^{20} (3.0×10^{20}) ($\Omega \text{ m}$)⁻¹ at an energy level of around -2.5 (-2.2) eV. Another notable value of σ is 2.36×10^{20} (1.96×10^{20}) ($\Omega \text{ m}$)⁻¹ at an energy of around 3.5 (3.84) eV. In the case of Pb_2MgTeO_6 , a high value of intensity of 3.5×10^{20} (2.50×10^{20}) ($\Omega \text{ m}$)⁻¹ is observed in the negative region, near -1.2 (-1.04) eV, and on the other hand, of 1.46×10^{20} (1.64×10^{20}) ($\Omega \text{ s}$)⁻¹ in the positive region at 3.94 (0.59) eV. These findings suggest that holes play a significant role as transporters in the $Pb_2Mg(W/Te)O_6$ materials. Increasing temperatures are shown to increase the value of σ (Fig. 4f). An increase in the value of σ at higher temperatures can be explained by the creation of more electrons due to bond unraveling at increasing temperatures.

Figure 4c and g displays the theoretical thermal conductivity (κ_{el}) as an estimate of μ [eV] and T [K], respectively. The trend of κ_{el} bears a similarity to σ . However, it has maximum values around

($9.43 \times 10^{15}/6.89 \times 10^{15}$) W/(mK) $\sim -2.24/-0.68$ eV and ($2.7 \times 10^{15}/2.3 \times 10^{15}$) W/(mK) ~ 4 eV were observed for Pb_2MgTeO_6 material with (GGA/HSE06). Similarly, for the Pb_2MgWO_6 material, the respective values are ($7.9 \times 10^{15}/6.87 \times 10^{15}$) W/(mK) at $-2.4/-2.0$ eV and ($6.3 \times 10^{15}/3.9 \times 10^{15}$) W/(mK) at 4 eV. Moreover, the dependence κ_{el} versus temperature T shows that the thermal conductivity parameter steadily increases at a rise rate, as compared to electrical conductivity.

The power factor PF quantifies the thermoelectric potency in the absence of thermal influences, as depicted in Fig. 4d, h. The GGA and HSE06 methods show strong peaks in the negative and positive direction of the chemical potential, indicating that hole and electron transport increase the thermoelectric intensity of these materials. For the Pb_2MgTeO_6 compound, the optimal values obtained with the GGA and HSE06 method are

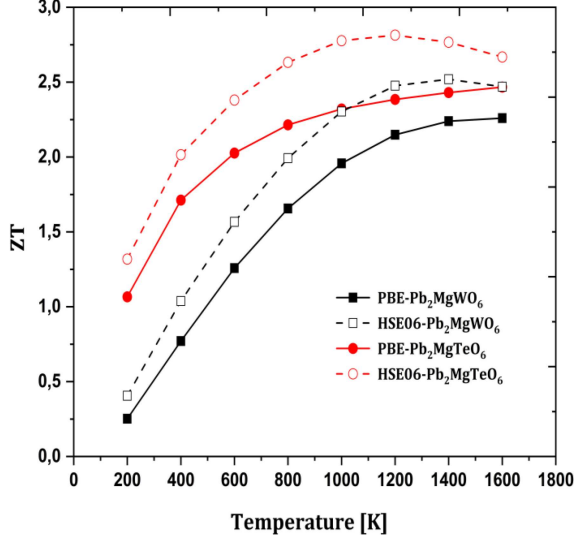


Fig. 5. Calculated values of the figure of merit for the Pb_2MgWO_6 and $\text{Pb}_2\text{MgTeO}_6$ compounds.

1.75×10^{12} W/(mK) and 1.44×10^{12} W/(mK), respectively. In contrast, for Pb_2MgWO_6 , the PF values are 1.56×10^{12} W/(mK) and 1.49×10^{12} W/(mK).

In order to achieve the desirable thermoelectric properties, it is imperative to ensure that the weighted mobility and bandgap exhibit high values. Furthermore, it is worth noting that the parameter ZT exhibits a correlation with the bandgap. For $\text{Pb}_2\text{Mg}(\text{Te/W})\text{O}_6$, the variation of ZT with temperature is presented in Fig. 5. It shows that the figure of merit ZT exhibits a clear correlation with the bandgap. The calculated values of optimal ZT at 1600 K using the GGA (HSE06) approximation are 2.46 (2.67) and 2.26 (2.47), respectively, for the compounds $\text{Pb}_2\text{MgTeO}_6$ and Pb_2MgWO_6 .

3.5. Optical properties

To understand the electronic structure of a substance and evaluate its suitability in optoelectronic applications, in this research we investigate the specific optical properties of the double perovskite materials under consideration, such as dielectric constants $\varepsilon(\omega)$, reflectivity $R(\omega)$, absorption coefficient $\alpha(\omega)$, extinction coefficient $K(\omega)$, and refractive index $n(\omega)$ related to energy E [eV] from the electromagnetic spectrum.

In Table IV, the optical properties of both compounds under consideration are outlined. The computed static dielectric constants of $\text{Pb}_2\text{Mg}(\text{W/Te})\text{O}_6$ double perovskites in ascending order of GGA and HSE06 are (22.4/8.14) and (1.76/1.8), respectively. Figure 6a demonstrates that for $\text{Pb}_2\text{Mg}(\text{W/Te})\text{O}_6$ compounds, the bandgap and static dielectric constant are inversely

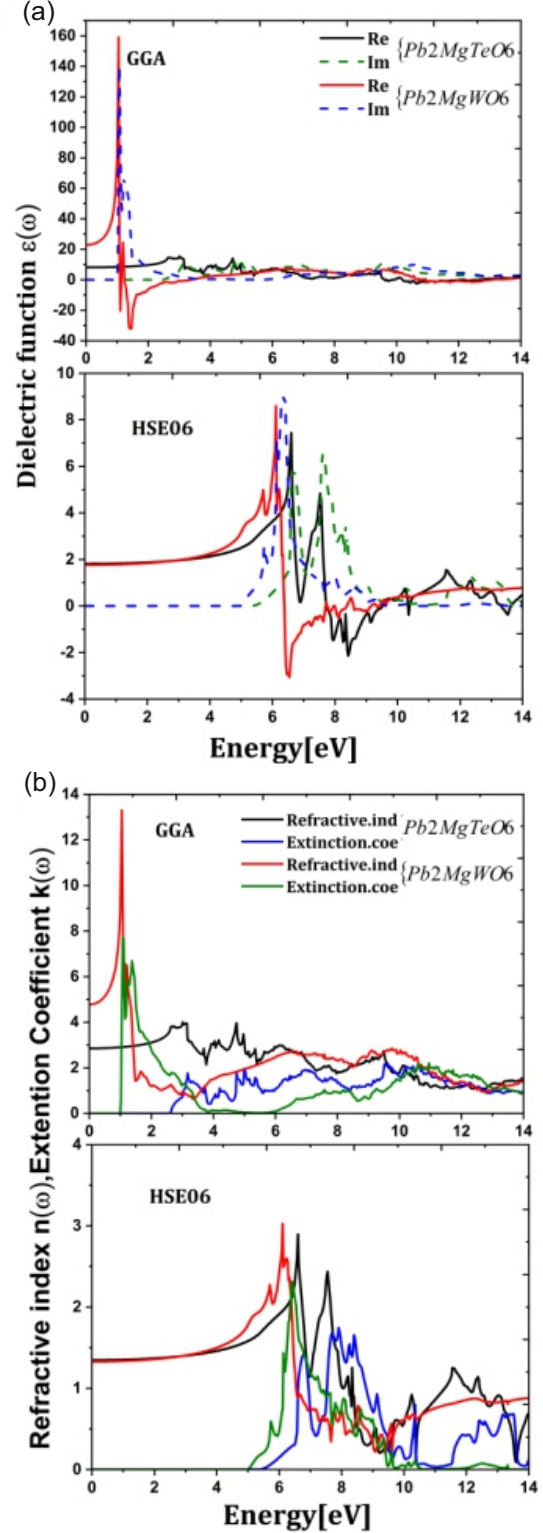


Fig. 6. Calculated optical parameters: (a) dielectric function, (b) complex refracted indexes.

related [52]. Where they have a far larger effect on GGA than on the HSE06 estimate, the intensity of the imaginary part of all compounds varies in height. Approximated by the HSE06 for

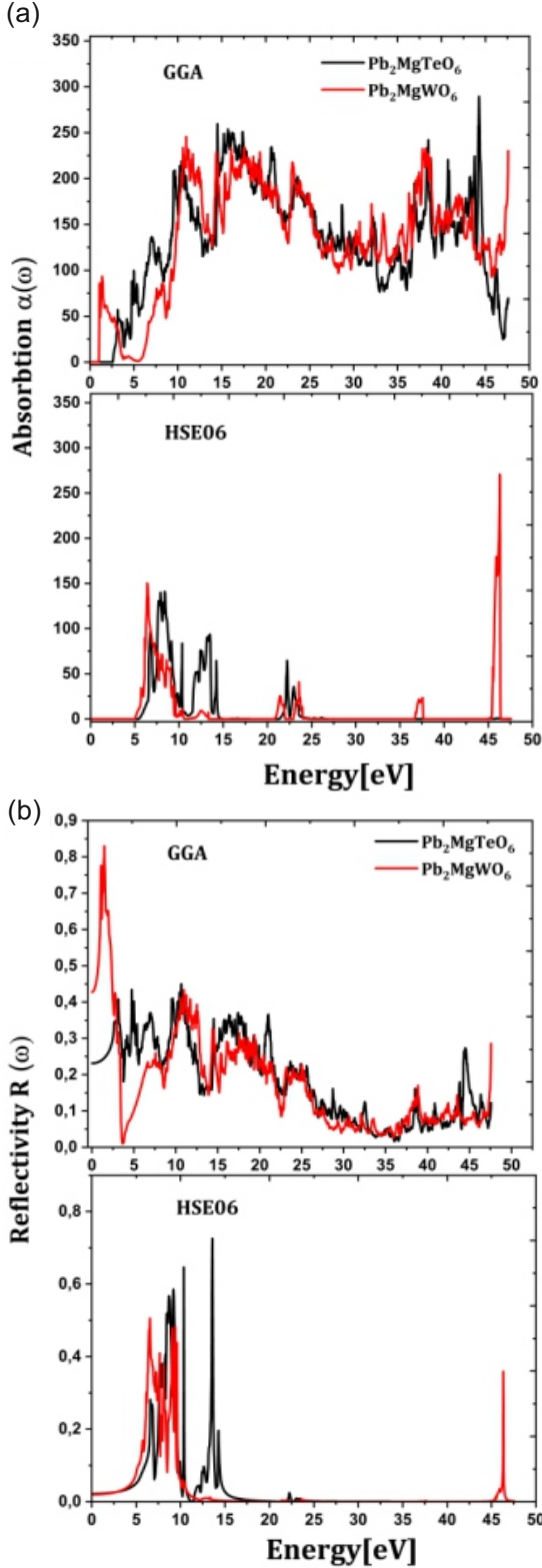


Fig. 7. Calculated optical parameters: (a) absorption, (b) reflectivity.

Pb_2MgTeO_6 , the main peaks are located within the photon energy 6.68 eV, whereas for Pb_2MgWO_6 — at 6.38 eV. With the GGA method, the peaks

TABLE IV

The calculated static parameters of Pb_2MgXO_6 ($X = W$ and Te) with GGA and HSE06.

		Static dielectric constant $\epsilon_1(0)$	Static refractive index $n(0)$	Reflectivity $R(0)$
Pb_2MgWO_6	PBE	22.84	4.78	0.42
	HSE06	1.76	1.33	0.02
Pb_2MgTeO_6	PBE	8.14	2.85	0.23
	HSE06	1.81	1.34	0.02

are located at 3.14 and 1.07 eV, respectively. The resulting shape agrees with the measured bandgap for all the measured [52].

The complex refracted indexes of materials can be characterized as $\tilde{n}(\omega) = n(\omega) + ik(\omega)$, in which $n(\omega)$ is the refractive index and $k(\omega)$ is the extinction coefficient. By comparing Fig. 6b with Fig. 6a, we can observe that the patterns exhibited by $n(\omega)$ and $k(\omega)$ are closely equivalent to those exhibited by $\epsilon_1(\omega)$ and $\epsilon_2(\omega)$. The computed refractive indexes at the zero photon energy according to (GGA/HSE06) approximations are (4.78/1.32) for Pb_2MgWO_6 and (2.85/1.34) for Pb_2MgTeO_6 . The values of $n(\omega)$ are indeed gradually increased in the (infrared/visible) light region and ultraviolet region with GGA and HSE06, respectively, reaching the upper values of (13.3/3.02) and (3.99/2.89). It is important to note that there is no available experimental data for comparison in this context.

In order to determine the optimal solar energy transformation effectiveness of a material, it is necessary to examine its absorption coefficient. According to the GGA approximation, the compounds have a high adsorption region in the energy ranges above 3.2 eV, reaching the greatest value of 232 (at 38 eV) and 229 (at 46 eV), respectively, for Pb_2MgWO_6 and Pb_2MgTeO_6 . On the other hand, when using the HSE06 approximation, the highest peaks are 270 (at 46 eV) and 139 (at 8 eV) (see Fig. 7a). Note that in the HSE06 approximation, the absorption spectra of Pb_2MgTeO_6 completely flatten as photon energy rises. It signifies that the materials exhibit strong reactions to radiation of ultraviolet energy and can operate effectively within this context.

One more interesting factor is reflectivity, which describes the difference between the amount of light energy that goes through a medium and the amount that is reflected from it. The computed values of R at zero photon energy are listed in Table IV. The materials have minor reflectivity ($\sim 10^{-1}$ with GGA and 10^{-2} with HSE06) (see Fig. 7b). Both of the $Pb_2Mg(W/Te)O_6$ perovskite

compounds exhibit a lower degree of reflectivity in the lower photon energy range, suggesting absorptivity and/or transmission in the materials.

4. Conclusions

In conclusion, first-principles DFT calculations were done using PBE-GGA exchange and correlation approximations and hybrid functionals (HSE06). We have obtained interesting characteristics of the Pb_2MgWO_6 and $\text{Pb}_2\text{MgTeO}_6$ compounds. Structural studies show that materials are stable in the cubic phase, supporting previous experimental data. The perovskite compounds Pb_2MgWO_6 and $\text{Pb}_2\text{MgTeO}_6$ exhibit semiconductor behavior with both GGA and HSE06 approaches, characterized by a direct bandgap of 2.36 (3.65) eV and 2.78 (4.21) eV, respectively. The optical characteristics of the researched perovskites suggest that they are appropriate for solar cell applications. The materials exhibit significant thermopower, with the transfer of thermoelectricity mostly attributed to their number of holes. Hence, the utilization of Pb_2MgWO_6 and $\text{Pb}_2\text{MgTeO}_6$ compounds is deemed suitable for their application in thermoelectric and optoelectronic devices.

References

- [1] E.W. Pickett, D.J. Singh, *Phys. Rev. B* **53**, 1146 (1996).
- [2] K.I. Kobayashi, T. Kimura, H. Sawada, K. Terakura, Y. Tokura, *Nature* **395**, 677 (1998).
- [3] K.H. Hellwege, A.M. Hellwege, *Magnetic and Other Properties of Oxides and Related Compounds*, Springer, 1970.
- [4] B.N. Parida, N. Panda, R. Padhee, R.K. Parida, *Phase Transit.* **91**, 638 (2018).
- [5] P.N. Lekshmi, G.R. Raji, M. Vasundhara, M.R. Varma, S.S. Pillai, M. Valant, *J. Mater. Chem. C* **2013**, 6565 (2013).
- [6] R. Nechache, C. Harnagea, L.-P. Carignan, O. Gautreau, L. Pintilie, M.P. Singh, D. Ménard, P. Fournier, M. Alexe, A. Pignolet, *J. Appl. Phys.* **105**, 061621 (2009).
- [7] S. Vasala, M. Karppinen, *Prog. Solid State Chem.* **43**, 1 (2015).
- [8] J. Brant, *Nat. Rev. Chem.* **2**, 393 (2018).
- [9] J. Kaczowski, M. Pugaczowa-Michalska, I. Płowaś-Korus, *J. Magn. Magn. Mater.* **548**, 168984 (2022).
- [10] D. Han, C. Feng, M.H. Du, T. Zhang, S. Wang, G. Tang, H. Ebert, *J. Am. Chem. Soc.* **143**, 12369 (2021).
- [11] H.A. Evans, L. Mao, R. Seshadri, A.K. Cheetham, *Annu. Rev. Mater. Res.* **51**, 351 (2021).
- [12] F.K. Patterson, C.W. Moeller, R. Ward, *Inorg. Chem.* **2**, 196 (1963).
- [13] F. Zhao, Z. Yue, Z. Gui, L. Li, *Jpn. J. App. Phys.* **44**, 8066 (2005).
- [14] M. Anderson, K. Greenwood, G. Taylor, K.R.B. Poeppelmeier, *Prog. Solid State Chem.* **22**, 197 (1993).
- [15] P.W. Barnes, M.W. Lufaso, P.M. Woodward, *Acta. Crystallog. B Struct. Sci.* **62**, 384 (2006).
- [16] W.J. Yin, B. Weng, J. Ge, Q. Sun, Z. Li, Y. Yan, *Energy Environ. Sci.* **12**, 442 (2019).
- [17] Y. Tokura, *Rep. Prog. Phys.* **69**, 797 (2006).
- [18] D.D. Sarma, P. Mahadevan, T. Saha-Dasgupta, S. Ray, A. Kumar, *Phys. Rev. Lett.* **85**, 2549 (2000).
- [19] Z. Hiroi, J. Yamaura, K. Hattori, *J. Phys. Soc. Jpn.* **81**, e0012 (2012).
- [20] K.W. Lee, W.E. Pickett, *Phys. Rev. B* **77**, 115101 (2008).
- [21] N.S. Rogado, J. Li, W.A. Sleight, M.A. Subramaniam, *Adv. Mater.* **17**, 2225 (2005).
- [22] J.P. Philipp, D. Reisinger, M. Schonecke, A. Marx, A. Erb, L. Alff, R. Gross, J. Klein, *Appl. Phys. Lett.* **79**, 3654 (2002).
- [23] M.A. Vries, A.C. McLaughlin, J.W.G. Bos, *Phys. Rev. Lett.* **104**, 177202 (2010).
- [24] G. Baldinozzi, P. Sciau, I. Moret, P.A. Buffat, *Solid State Commun.* **89**, 441 (1994).
- [25] G. Baldinozzi, D. Grebille, P. Sciau, J.M. Kiat, J. Moret, J.F. Berar, *J. Phys. Condens. Matter* **10**, 6461 (1998).
- [26] R. Caracas, X. Gonze, *Phys. Rev. B* **65**, 184103 (2002).
- [27] R. Caracas, X. Gonze, *Phys. Rev. B* **71**, 054101 (2005).
- [28] G. Baldinozzi, P.H. Sciau, *Acta. Cryst. B* **51**, 668 (1995).
- [29] G. Baldinozzi, P. Sciau, P.A. Buffat, *Solid State Commun.* **86**, 541 (1993).
- [30] P. Blaha, K. Schwarz, K.S.B. Trickey, *Comput. Phys. Commun.* **59**, 399 (1990).
- [31] G.K.H. Madsen, P. Blaha, K. Schwarz, E. Sjöstedt, L. Nordström, *Phys. Rev. B* **64**, 195134 (2001).
- [32] P. Hohenberg, W. Kohn, *Phys. Rev.* **136**, e00B864 (1964).

- [33] M. Städele, J.A. Majewski, P. Vogl, *Phys. Rev. Lett.* **79**, 2089 (1997).
- [34] J. Heyd, G.E. Scuseria, M. Ernzerho, *J. Chem. Phys.* **118**, 8207 (2003).
- [35] M. Jamal, S.J. Asadabadi, I. Ahmad, H.A.R. Aliabad, *Comput. Mater. Sci.* **95**, 592 (2014).
- [36] D. Singh, M. Sajjad, J.A. Larsson, R. Ahuja, *Results Phys.* **19**, 103584 (2020).
- [37] V. Goldschmidt, *Geochemistry*, Oxford University Press, 1958.
- [38] F.S. Galasso, *Structure, Properties and Preparation of Perovskite-type Compounds*, Pergamon Press, London 1969.
- [39] W. Westerburg, O. Lang, C. Ritter, C. Felser, W. Tremel, G. Jakob, *Solid State Commun.* **122**, 201 (2002).
- [40] F. Sania, S. Shafie, *IOSR-JEEE* **14**, 51 (2019).
- [41] G. Volonakis, A. Haghighirad, R. Milot, W. Sio, M. Filip, B. Wenger, M. Johnston, L. Herz, H. Snaith, F. Giustino, *J. Phys. Chem. Lett.* **8**, 772 (2017).
- [42] R.D. Shannon, C.T. Prewitt, *Acta. Cryst.* **B25**, 925 (1969).
- [43] M. Born, K. Huang, *Dynamical Theory of Crystal Lattices*, Clarendon Press, Oxford 1956.
- [44] A. Yakoubi, O.Baraka, B. Bouhafs, *Results Phys.* **2**, 58 (2012).
- [45] S.F. Pugh, *Lond. Edinb. Philos. Mag. J. Sci.* **45**, 823 (1954).
- [46] I.N. Frantsevich, F.F. Voronov, S.A. Bakuta, *Elastic Constants and Elastic Moduli of Metals and Nonmetals*, Naukova Dumka, Kiev 1982.
- [47] Y. Tian, B. Xu, Z. Zhao, *Int. J. Refract. Metal. Hard Mater.* **33**, 93 (2012).
- [48] O.L. Anderson, *J. Phys. Chem. Solids* **24**, 909 (1963).
- [49] M.E. Fine, L.D. Brown, H.L. Marcus, *Scr. Metall.* **18**, 951 (1984).
- [50] G. Giorgi, J.I. Fujisawa, H. Segawa, K. Yamashita, *J. Phys. Chem. Lett.* **4**, 4213 (2013).
- [51] M. Sajjad, N. Singh, S. Sattar, S.D. Wolf, U. Schwingenschlogl, *ACS. Appl. Energy Mater.* **2**, 3004 (2019).
- [52] D.R. Penn, *Phys. Rev.* **128**, 2093 (1962).